



MgO-incorporated porous nanofibrous scaffold promotes osteogenic differentiation of pre-osteoblasts



Xiaoyu Wang^a, Mingyue Liu^a, Haiyan Li^a, Anlin Yin^b, Changlei Xia^c, Xiangxin Lou^a, Hongsheng Wang^a, Xiumei Mo^a, Jinglei Wu^{a,*}

^a Key Laboratory of Science and Technology of Eco-Textile & Shanghai Engineering Research Center of Nano-Biomaterials and Regenerative Medicine, College of Chemistry, Chemical Engineering and Biotechnology, Donghua University, Shanghai 201620, China

^b College of Material and Textile Engineering, Jiaying University, Jiaxing, Zhejiang 314001, China

^c Co-Innovation Center of Efficient Processing and Utilization of Forestry Resources, College of Materials Science and Engineering, Nanjing Forestry University, Nanjing, Jiangsu 210037, China

ARTICLE INFO

Article history:

Received 9 September 2020

Received in revised form 15 March 2021

Accepted 21 May 2021

Available online 24 May 2021

Keywords:

Biomaterials

Magnesium oxide nanoparticles

Biomimetic

Scaffold

Osteogenesis

ABSTRACT

A feasible approach to fabricate porous nanofibrous scaffolds structurally similar to native extracellular matrix was reported. Magnesium oxide (MgO) nanoparticles were incorporated into electrospun poly (lactic acid) (PLA)/gelatin membranes, which were processed into short fibers and reconstructed to three-dimensional scaffolds. The scaffold exhibited sponge-like appearance with interconnected pores ranging from 50 to 200 μm and was highly elastic. MgO nanoparticles hydrolyzed and alleviated the acidic degradation products of PLA/gelatin scaffold. Released magnesium ions were beneficial to pre-osteoblasts by promoting proliferation and by upregulating osteogenic differentiation, indicating that the scaffold might find opportunities for bone grafting materials.

© 2021 Elsevier B.V. All rights reserved.

1. Introduction

Bone defects caused by trauma, tumor resection, and aged-related diseases frequently occur, and the management of large bone defects remains a significant challenge. Current prosthetic implants made from metals, ceramics, and plastics come with several inherent limitations such as stress shielding and incapability of growth [1]. These implants might be problematic for young patients with growing body. Many efforts have been devoted to developing absorbable bone implants to circumvent this problem. Electrospun nanofibers share many similarities with the extracellular matrix (ECM) of bone, while conventional electrospinning gives to dense membranes/mats with limited thickness, which limits their potential as bone grafting materials [2].

Recently, post-electrospinning treatments to increase the porosity and dimensionality of electrospun scaffolds have expanded their applicability for bone regeneration [3]. We and other groups reported similar fantastic techniques to manipulate densely compacted electrospun nanofibers to individual short fibers and then reconstruct them into highly porous scaffolds

[1,4]. These scaffolds have interconnected pore structure with nanofibrous surface texture, which perfectly resembles the ECM of bones. Our recent study also demonstrated that incorporating magnesium oxide (MgO) nanoparticles into electrospun nanofibrous membranes greatly enhances its osteogenic activity [5]. In this study, MgO nanoparticles were incorporated into electrospun nanofibers and subsequently manipulated to 3D porous scaffolds. MgO-incorporated scaffolds exhibited good cytocompatibility and elevated osteogenic differentiation of pre-osteoblasts.

2. Experimental

2.1. Scaffold preparation

MgO-incorporated nanofibrous scaffold was prepared according to our previous studies with modifications [4,5]. Poly(lactic acid) (PLA, Mw 50 kDa, Jinan Daigang Biomaterial Co., Ltd) and Type A gelatin (Sigma) were dissolved in 1,1,1,3,3,3-hexafluoro-2-propanol (Shanghai Darui Finechemical Co., Ltd) at the concentration of 11% (wt/v) with a PLA/gelatin mass ratio of 1:5. MgO nanoparticles (~50 nm diameter, Shanghai Aladdin) were added to the PLA/gelatin solution at a concentration of 2.5 mg/mL (wt/v) and sonicated for 30 min to allow homogeneous dispersion. The

* Corresponding author.

E-mail address: jw@dhu.edu.cn (J. Wu).

PLA/gelatin/MgO preparation was fed at 3 mL/h and electrospun at 15 kV to obtain nanofibrous membranes. Membranes were tailored into 10 mm squares for mechanical homogenization. Samples (3 g) were revolved to individual short fibers in *tert*-butanol (100 mL) by an IKA T18 homogenizer at 10,000 rpm for 30 min. Suspended short fibers were cast to cylindrical molds, frozen at $-20\text{ }^{\circ}\text{C}$, and lyophilized to reconstruct into porous nanofibrous scaffolds. Subsequently, crosslinking of scaffolds was performed by two cycles of heat-treating at $190\text{ }^{\circ}\text{C}$ for 2 h to increase their structural

stability [4]. PLA/gelatin scaffolds without MgO were prepared by the same method and served as control.

2.2. Characterization, cytocompatibility, and osteogenic activity of scaffolds

The scaffolds were sputter-coated with platinum for the visualization of nanofibrous morphology and porous architecture by field-emission scanning electron microscopy (SEM, Hitachi,

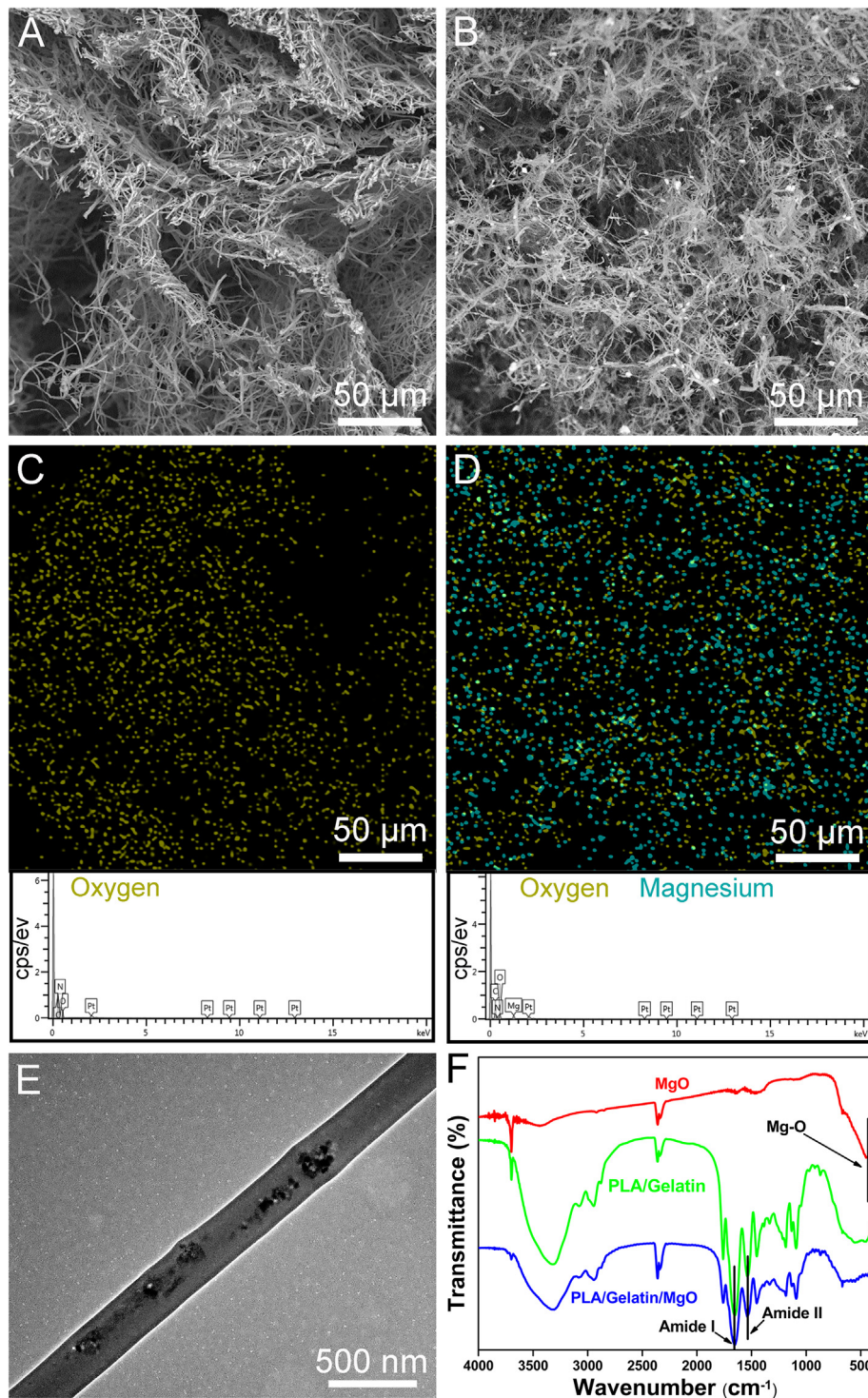


Fig. 1. SEM (A and B) and EDS (C and D) mapping images with EDX spectra show fibrous ultrastructure and elemental compositions (oxygen: yellow; magnesium: blue) of PLA/gelatin (A and C) and PLA/gelatin/MgO (B and D) scaffolds, respectively. TEM image verifies the presence of MgO nanoparticles within nanofibers (E). FTIR spectra show characteristic absorbance peaks of scaffold components and scaffolds (F).

TM-1000, Japan) equipped with X-ray energy dispersive spectroscopy (EDS). The pore size of scaffolds was measured from the SEM images using Image J. The presence of MgO nanoparticles within nanofibers was verified by transmission electron microscopy (TEM, Hitachi, H-800, Japan). Compositional analysis was performed by an attenuated total Fourier transform infrared spectroscopy (FTIR, Nicolet-760, Madison, WI) over the range of 400–4000 cm^{-1} .

The determination of magnesium ion release and pH variation of scaffolds was performed by incubating samples in 0.9% saline. pH values of incubations were measured at predesigned time points ($n = 4$). Magnesium ion was determined by an inductively coupled plasma atomic emission spectroscopy (ICP-AES) (Prodigy Plus, Teledyne Leeman Labs, USA) ($n = 4$). A 50-cycle loading–unloading fatigue test was performed by measuring a compression strain of 60% at the compressing speed of 5 mm/min using a materials testing machine (Instron 5567, Norwood, MA). Samples were hydrated with saline at 37 °C prior to the test ($n = 4$).

Scaffolds were cut into discs (11 mm diameter), disinfected by ultraviolet radiation overnight prior to cell seeding. MC3T3-E1 pre-osteoblast cell line was provided by the Cell Bank of the Chinese Academy of Sciences and expanded in α -MEM with 10% fetal

bovine serum and 1% antibiotics. Each scaffold was seeded with 2×10^5 cells and cultured for 2 weeks. Cells were visualized after fluorescence live/dead staining and then fixed in 4% paraformaldehyde, dehydrated with gradient ethanol, sopper-coated with gold, and observed by SEM. The osteogenic activity of scaffolds was evaluated by alkaline phosphatase (ALP) activity analysis using an ALP assay kit (Beyotime Biotechnology) ($n = 4$).

2.3. Statistical analysis

Data were present as mean \pm standard deviation. Statistical analyses were performed by unpaired Student's *t*-test. Statistical significance was considered at $p < 0.05$.

3. Results and discussion

Uncrosslinked scaffolds showed white color, while they maintained porous texture and became light yellow after heating treatment (Fig. S1). The PLA/gelatin (Fig. 1A) and PLA/gelatin/MgO (Fig. 1B) scaffolds showed nanofibrous ultrastructure with open pores (~ 50 – $200 \mu\text{m}$). Pores of the PLA/gelatin scaffold were defined

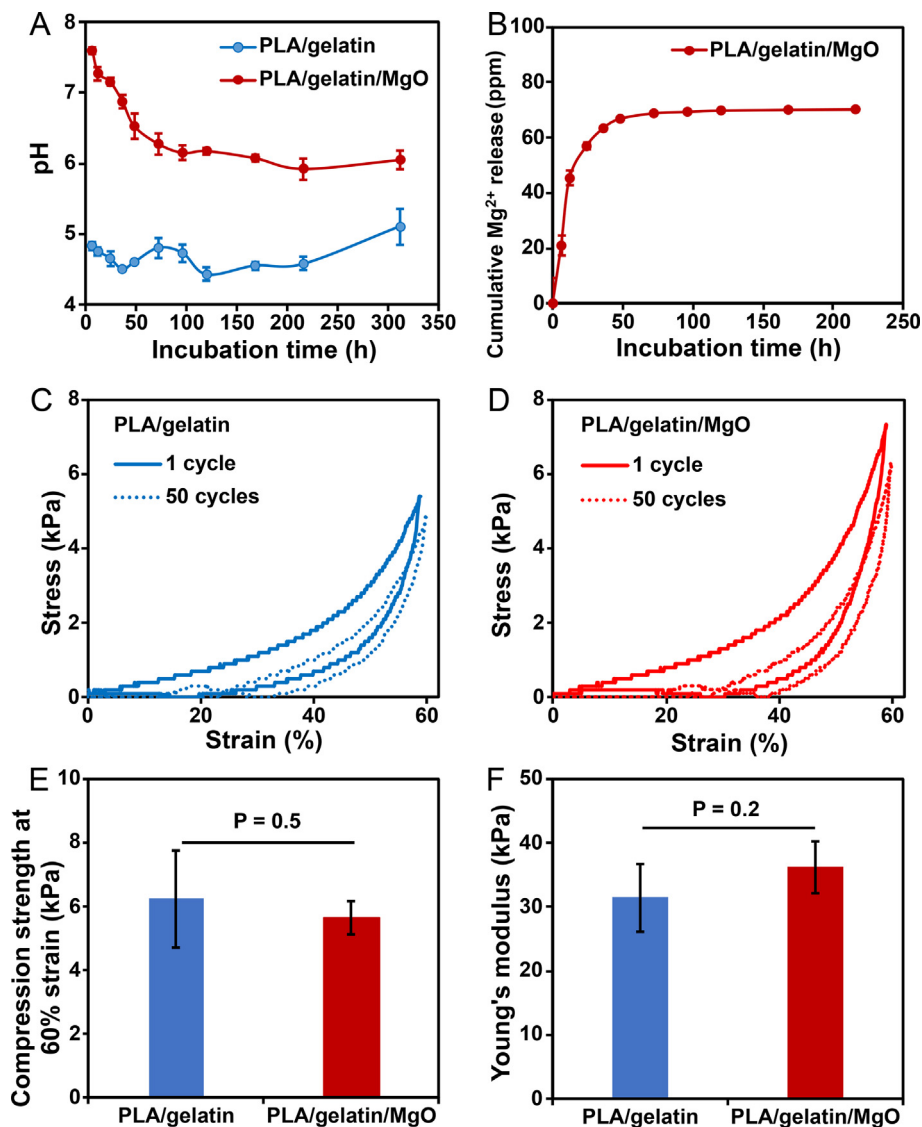


Fig. 2. pH variation (A) and magnesium release (B) of scaffolds incubated in saline. Cyclic compression curves (C and D), compression strength at 60% strain (E), and Young's modulus (F) of scaffolds. Unpaired two-tailed Student's *t*-test.

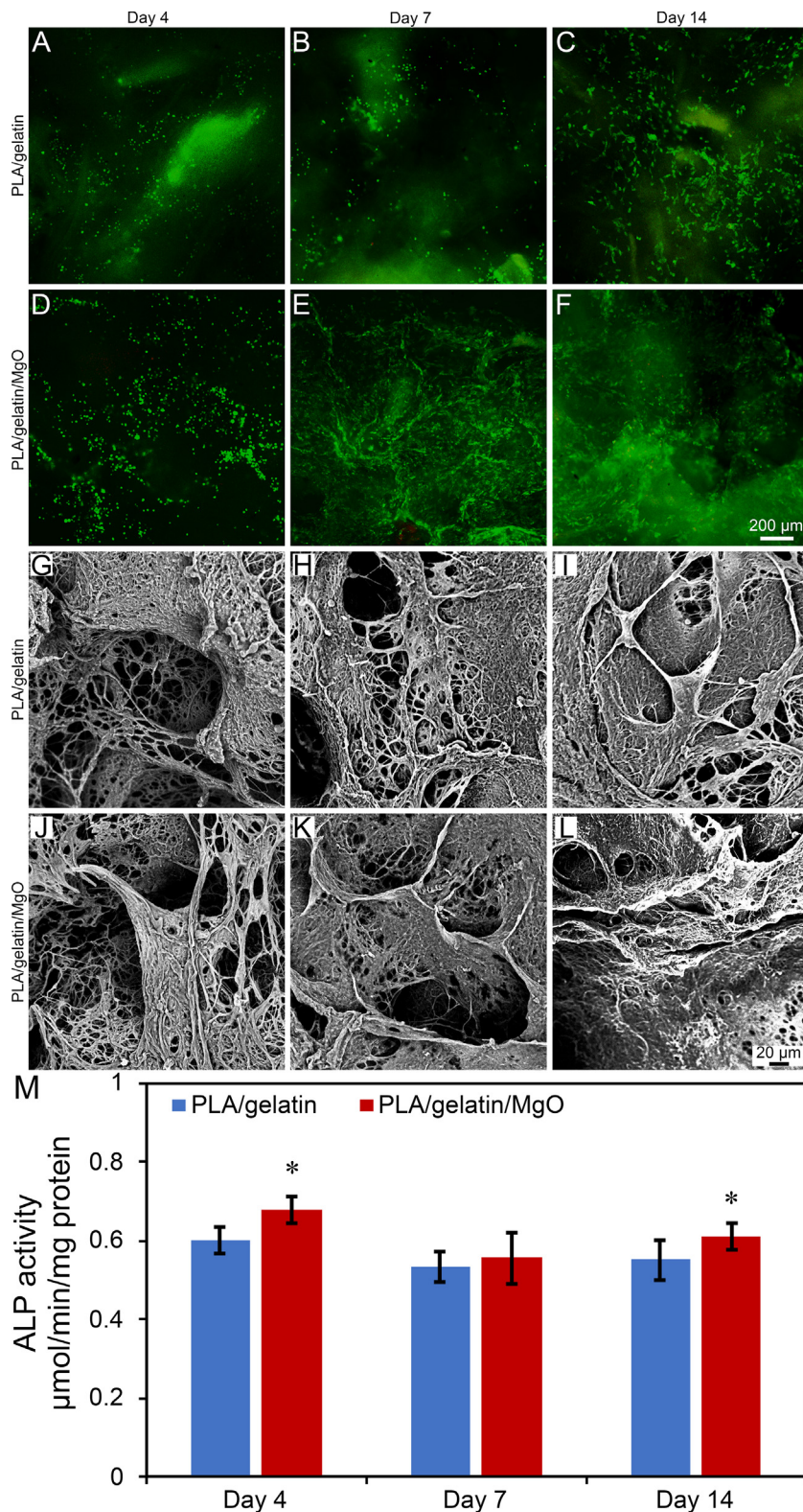


Fig. 3. Live/dead (A-F) and SEM (G-L) images of MC3T3-E1 cells on PLA/gelatin (A-C and G-I) and PLA/gelatin/MgO (D-F and J-L) scaffolds up to 14 days. The PLA/gelatin/MgO scaffold elevates the ALP activity of MC3T3-E1 cells (M). Unpaired one-tailed Student's *t*-test, * versus PLA/gelatin, $p < 0.05$.

by compacted nanofiber sheets. The PLA/gelatin/MgO scaffold had a reduced degree of fiber compression and exhibited more uniform pores with better interconnection. This result indicates that the presence of MgO nanoparticles with the PLA/gelatin nanofibers

decreases fiber bonding during thermal-induced crosslinking. Our previous study also found a similar phenomenon that hydroxyapatite nanoparticle incorporated nanofibrous scaffolds exhibited a less compacted fibrous configuration [6]. This is

probably due to the increased brittleness of PLA/gelatin nanofibers induced by inorganic nanoparticles, which makes nanofibers less flexible and more resistant to thermal-induced fiber–fiber bonding.

EDS mapping images revealed that magnesium element was absent in the PLA/gelatin scaffold (Fig. 1C), while it was homogeneously distributed within the PLA/gelatin/MgO scaffold (Fig. 1D). Magnesium constituted 3.32% total weight (Table S1), indicating that the PLA/gelatin/MgO scaffold contains 5.5% (wt/wt) MgO. TEM image verified that MgO nanoparticles were predominately present in the form of individual particles within PLA/gelatin/MgO nanofibers (Fig. 1E), though occasional aggregation of MgO nanoparticles was observed (Fig. 1B). Because MgO nanoparticles are not soluble in *tert*-butanol and are embedded in the center of nanofibers, they are less vulnerable to mechanical disturbance during homogenization and subsequent treatments. FTIR spectra showed characteristic absorbance peaks of amide I and amide II of scaffolds, as well as a broad band at 437 cm^{-1} associated with Mg-O vibration of MgO nanoparticles (Fig. 1F). Mg-O vibration was not observed in the PLA/gelatin/MgO scaffold, probably due to the strong peaks of organic matter that flatten the inorganic matter.

The PLA/gelatin scaffold exhibited weak acidic nature and results in a pH of around 5 when incubating in saline (Fig. 2A). Incorporation of MgO nanoparticles into scaffolds elevated the pH to above 7 at the early time points, which subsequently went down to below 7 but was still higher than the PLA/gelatin scaffold. Magnesium release mainly occurred within the first two days as quantified by ICP-AES (Fig. 2B). This indicates that the hydrolysis of MgO nanoparticles partially neutralizes the acidic degradation products of PLA [5]. The PLA/gelatin (Fig. 2C) and PLA/gelatin/MgO (Fig. 2D) scaffolds showed similar cyclic compression curves with equivalent compression strengths (Fig. 2E) at 60% strain and Young's moduli of $\sim 30\text{ kPa}$ (Fig. 2F). Previous studies have demonstrated that Mg inorganic particles showed dose-dependent effects on the mechanical properties of composite scaffolds [5,7,8]. Appropriate amounts of MgO nanoparticles (<1%) allow homogenous distribution of those particles within electrospun nanofibers and transfer stress between polymer chains, contributing to improved mechanical properties [5]. We did not observe increased compression strength for the PLA/gelatin/MgO scaffold. This is likely related to the short nanofiber configuration that cannot continuously transfer forces.

MC3T3-E1 cells maintained a round shape from day 4 (Fig. 3A) to 7 (Fig. 3B) on PLA/gelatin scaffolds. Cells transformed to spindle shape and were greatly colonized at day 14 (Fig. 3C). Cells showed morphology change from round shape at day 4 (Fig. 3D) to spindle shape at day 7 on the PLA/gelatin/MgO scaffold (Fig. 3E), which was much faster than that on the PLA/gelatin scaffold. Individual cells attached to the fibers either with a round (Fig. 3G) or flattened (Fig. 3J) shape. Cells showed increased confluence at day 7 (Fig. 3H and K) and almost covered the scaffold surface at day 14 (Fig. 3I and L). Both scaffolds maintained highly porous structures during *in vitro* culture. MC3T3-E1 cells showed significantly greater ALP activity on the PLA/gelatin/MgO scaffold compared with that on the PLA/gelatin at day 4 (Fig. 3M). Although ALP activity tended to decrease thereafter, the PLA/gelatin/MgO scaffold exhibited greater capacity in promoting ALP activity of MC3T3-E1 cells at day 14. These results demonstrated that incorporated MgO

nanoparticles within scaffolds not only boost the proliferation of MC3T3-E1 cells but also promote their osteogenic differentiation.

4. Conclusions

We demonstrate that MgO nanoparticle-incorporated scaffold exhibits nanofibrous ultrastructure with open-pores and alike to native ECM. Incorporated MgO nanoparticles mitigate the acidic environment of PLA-based scaffold. The scaffold shows good cytocompatibility and elevates osteogenic differentiation of pre-osteoblasts, suggesting its feasibility as implant materials for bone repair and regeneration.

CRedit authorship contribution statement

Xiaoyu Wang: Conceptualization, Methodology, Formal analysis, Investigation, Formal analysis, Writing - original draft. **Min-gyue Liu:** Methodology, Formal analysis. **Haiyan Li:** Methodology, Formal analysis. **Anlin Yin:** Conceptualization, Investigation, Writing - review & editing. **Changlei Xia:** Formal analysis. **Xiangxin Lou:** Resources, Formal analysis. **Hongsheng Wang:** Resources, Formal analysis, Methodology. **Xiumei Mo:** Resources, Writing - review & editing. **Jinglei Wu:** Conceptualization, Validation, Investigation, Resources, Supervision, Writing - original draft, Writing - review & editing.

Declaration of Competing Interest

The authors declare that they have no known competing financial interests or personal relationships that could have appeared to influence the work reported in this paper.

Acknowledgments

Authors acknowledge support from Donghua University (2232019D3-20) and National Natural Science Foundation of China (31900949).

Appendix A. Supplementary data

Supplementary data to this article can be found online at <https://doi.org/10.1016/j.matlet.2021.130098>.

References

- [1] L. Weng, S.K. Boda, H. Wang, M.J. Teusink, F.D. Shuler, J. Xie, *Adv. Healthcare Mater.* 7 (2018) 10.
- [2] L. Deng, Y. Li, H. Zhang, *J. Biomed. Mater. Res. B Appl. Biomater.* 108 (4) (2020) 1505–1517.
- [3] J. Wu, Y. Hong, *Bioact. Mater.* 1 (1) (2016) 56–64.
- [4] W. Chen, S. Chen, Y. Morsi, H. El-Hamshary, M. El-Newhy, C. Fan, X. Mo, *A.C.S. Appl. Mater. Interfaces* 8 (37) (2016) 24415–24425.
- [5] X. Liu, X. He, D. Jin, S. Wu, H. Wang, M. Yin, A. Aldalbahi, M. El-Newehy, X. Mo, *J. Wu, Acta Biomater.* 108 (2020) 207–222.
- [6] K. Ye, D. Liu, H. Kuang, J. Cai, W. Chen, B. Sun, L. Xia, B. Fang, Y. Morsi, X. Mo, *J. Colloid Interface Sci.* 534 (2019) 625–636.
- [7] N.P. Rijal, U. Adhikari, S. Khanal, D. Pai, J. Sankar, N. Bhattarai, *Mater. Sci. Eng. B* 228 (2018) 18–27.
- [8] U. Adhikari, X. An, N. Rijal, T. Hopkins, S. Khanal, T. Chavez, R. Tatu, J. Sankar, K.J. Little, D.B. Hom, N. Bhattarai, S.K. Pixley, *Acta Biomater.* 98 (2019) 215–234.